Mem. S.A.It. Vol. 90, 497

Memorie della

Mapping the large scale CO-depletion in the IRDC G351.77-0.51

G. Sabatini[1,2,3], A. Giannetti[2], S. Bovino[3], J. Brand[2], S. Leurini[4], E. Schisano[5], T. Pillai[6,7], and K. M. Menten[6]

[1] Dipartimento di Fisica e Astronomia, Università degli Studi di Bologna, via Gobetti 93/2, I-40129 Bologna, Italy, e-mail: giovanni.sabatini4@unibo.it
[2] INAF - Istituto di Radioastronomia - Italian node of the ALMA Regional Centre (ARC), via Gobetti 101, I-40129 Bologna, Italy
[3] Departamento de Astronomía, Universidad de Concepción, Barrio Universitario, Concepción, Chile
[4] INAF - Osservatorio Astronomico di Cagliari, via della Scienza 5, 09047 Selargius (CA), Italy
[5] Istituto di Astrofisica e Planetologia Spaziali - INAF, Via Fosso del Cavaliere 100, I-00133 Roma, Italy
[6] Max-Planck-Institut für Radioastronomie, Auf dem Hügel 69, 53121 Bonn, Germany
[7] Institute for Astrophysical Research, 725 Commonwealth Ave, Boston University Boston, MA 02215, USA

Abstract. Knowledge of the degree of CO-depletion provides information on the physical conditions occurring in the innermost and the densest regions of molecular clouds. A key parameter is the radius within which the CO is depleted (R_{dep}). We present a study of the depletion of CO in the Infrared Dark Cloud G351.77-0.51 (G351), to derive the depletion across the cloud. We use the *Herschel* (Hi-Gal) and LABOCA dust continuum data, combined with APEX $C^{18}O$ and $C^{17}O$(2-1) line observations. We built a simple model to investigate the size of the CO-depleted region in G351. The model suggests that $R_{dep} < 0.15$ pc, where we estimate a hydrogen number density $> 2 \times 10^4$ cm^{-3}. These results provide crucial information on the spatial scales on which different chemical processes can operate in high-mass star forming regions.

Key words. Galaxy: depletion of CO – Galaxy: high-mass star-forming processes – Galaxy: star formation – Galaxy: infrared dark clouds – Galaxy: ISM & chemistry

1. Introduction

Infrared Dark Clouds (IRDCs) are recognized as the nurseries of massive stars (e.g. Menten et al. 2005 and Bergin & Tafalla 2007, hereafter BT07). They are dusty and dense (volume density $n(H_2)>$ a few $\times$ 10^4 cm^{-3}; e.g. Crapsi et al. 2005) filamentary structures of cold molecular gas, where temperatures are < 20 K (e.g. Caselli et al. 2008). They appear in absorption against the background emission at 8 μm, while observations at longer wavelengths, tracing the dust continuum *emission*, show their internal clumpiness revealing the cores where star-formation actually takes place (see Zinnecker & Yorke 2007 for more details).

If we compare dust continuum and molecular line emission from the same clump, we notice a discrepancy between the locations at which the two emissions peak. While the continuum emission peaks at the center, where we expect the highest density, the same is not necessarily true for the molecular lines. Nitrogen-bearing species follow the dust distribution, but the carbon-bearing species can show a lack of emission at the dust continuum peak (e.g. BT07).

The explanation of this behaviour is the so-called CO-depletion (e.g. Caselli et al. 1999). After the interaction between a CO molecule and a dust grain, the molecule can be captured onto the grain surface with a certain probability called sticking coefficient, S. This is what generates the deficiency of CO in the densest regions.

The characteristic time scale of this phenomenon is inversely proportional to the sticking coefficient and the volume density of H_2:

$$\tau_{dep} \sim \frac{10^9}{S\ n(H_2)}\ \text{yr}. \tag{1}$$

Low temperatures and high density favour the depletion of CO, facilitating also the formation of complex molecules on the dust grains via two-body reactions (e.g. Herbst & van Dishoeck 2009).

How much of the CO is depleted onto the surface of the dust grains is usually characterized by the depletion factor, defined as the ratio between the 'expected', $\chi^E_{\rm CO}$, and the observed, $\chi^O_{\rm CO}$, abundance of CO with respect to H_2 (e.g. Fontani et al. 2012):

$$f_D = \frac{\chi^E_{\rm CO}}{\chi^O_{\rm CO}}. \tag{2}$$

High-mass star-forming regions (HMSFRs) are potentially more prone to show large-scale depletion due to the high volume densities of H_2 in clumps and in the surrounding inter-clump medium (Giannetti et al. 2014).

In different samples of young HMSFRs, the observed depletion factor is found to vary between 1 and a few tens, but we should consider that these values are beam- and line-of-sight-averaged quantities. This means that along the line-of-sight there will be regions in which the CO could be completely in the gas phase (i.e $f_D = 1$) and others in which the depletion factor can reach values larger than those actually observed ($f_D \gtrsim 10$).

The physical size of the highly depleted region – the so called depletion radius, R_{dep}, i.e. the radius within which most of the C-bearing species, and in particular CO, are locked onto dust grains – is not known. This parameter is however important because it defines the spatial scale on which the relative importance of different chemical processes could change.

2. Observations

We selected the nearest and most massive source from the ATLASGAL survey (Schuller et al. 2009; Li et al. 2016), the IRDC G351.77-0.51 (hereafter G351), to derive an estimate of the magnitude of R_{dep}. This source's proximity and shape allow us to investigate the scales on which CO-depletion is efficient and at the same time to build an axisymmetric (toy-)model to compute R_{dep}.

Herschel observations in four different bands are available for this source and can be combined with the *LArge APEX BOlometer CAmera* (LABOCA) map of the 870 μm dust continuum emission. We performed a pixel-by-pixel fit to the spectral energy distribution to construct the dust temperature map (following Leurini et al. 2019, hereafter L19). In the brightest clump of G351 (labeled '1' in Fig. 1), the *Herschel* observations were saturated, so we masked the region of this hot-core. Following L19, we assumed an opacity law as defined in Hildebrand (1983), and from the surface density of dust, we generate the map of the column density of H_2, N(H_2), assuming a gas-to-dust mass ratio of 120 (Giannetti et al. 2017a).

Pointed observations of the (2-1) transitions of two CO isotopologues, $C^{17}O$ and $C^{18}O$, are also available, as well as an on-the-fly map of the same transition of $C^{18}O$. We generated the map of the column density of $C^{18}O$, N($C^{18}O$), assuming that its excitation temperature is proportional to the dust temperature (Giannetti et al. 2017b). We then applied

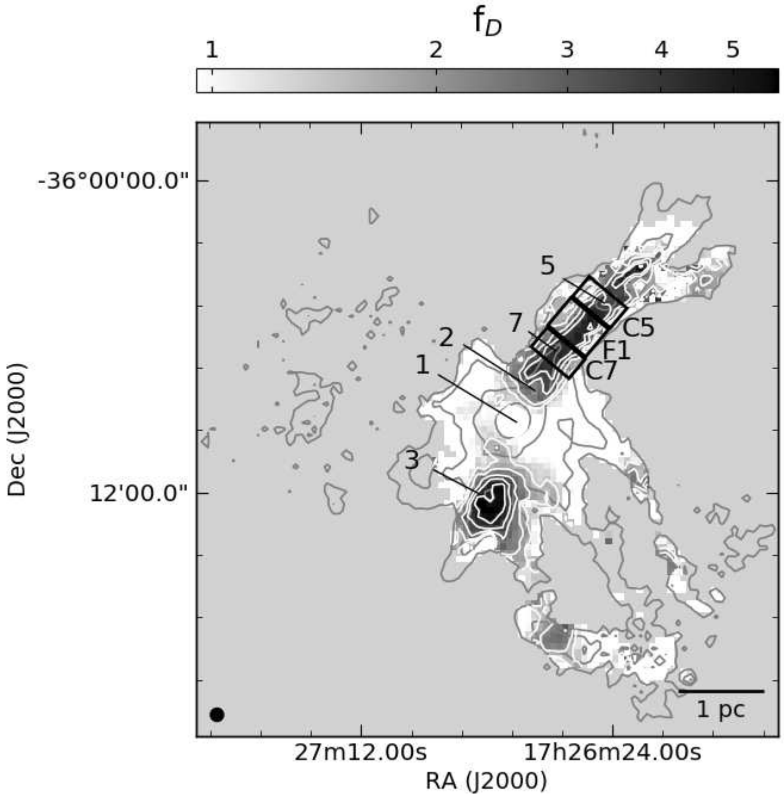

Fig. 1. Depletion factor (f_D) map obtained by taking the ratio between the expected and observed N($C^{18}O$). We assumed a canonical abundance of $2.1{\times}10^{-7}$ of N($C^{18}O$) relative to N(H_2). The grey contours mark the 3, 9, 27 and 81σ levels of the integrated emission of the APEX $C^{18}O$ J(2-1) line, where 3σ = 0.9 K km s^{-1}. The white contours are defined at f_D = 1.5, 2, 3, 4 and 5. Black rectangular regions (i.e. C5, C7 and F1) show where the models discussed in Sect. 4 were applied to estimate the size of R_{dep}. The plot is adapted from Sabatini et al. (2019) and reprinted with permission.

the classical approach described in Kramer & Winnewisser (1991), taking into account possible opacity effects. We derived $\tau_{C^{18}O}$ from the ratio of the main-beam brightness temperatures of the isotopologues and assuming their abundance ratio, Φ, to be equal to 4 (e.g. Wouterloot et al. 2008).

3. Large-scale CO-depletion map

The final depletion map is shown in Fig. 1. It was generated by taking $\chi^E_{C^{18}O} = 2.1{\times}10^{-7}$ (see Giannetti et al. 2017a). The clumps[1] (labels 1, 2, 3, 5 and 7) defined by Leurini et al. (2011b) appear well-pronounced along the main filamentary structure, which in L19 is labelled the "main-body".

In this cloud, the depletion factor ranges between 1 and 6, reaching its highest values along the main-body of G351. In Fig. 1 we see that CO-depletion affects not only the densest regions of the clumps but also the less prominent and filamentary structures that surround

[1] We show only the clumps for which data on both the CO isotopologues are available.

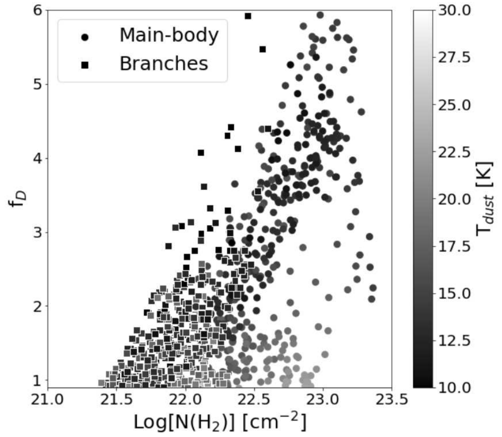

Fig. 2. Pixel-by-pixel scatter plot of the whole structure detected in Fig. 1. Circles represent the pixels of the main body, the squares those of the branches. The plot is adapted from Sabatini et al. (2019) and reprinted with permission.

them, as shown for the first time by Hernandez et al. (2012) in the IRDC G035.30-00.33.

This behaviour is also visible in Fig. 2, where a scatter plot shows how the final values of f_D vary as a function of n(H_2), and the dust temperature, T_{dust} (see Sabatini et al. 2019 for more details on how the maps were generated): circles and squares, respectively, are used to distinguish the pixels of the main-body from those of the sub-filamentary structures, hereafter "branches".

Along the branches, temperatures are $\lesssim$15 K, while the highest values ($\sim$30 K) are reached around the hot-core in clump-1, as expected from the intense star formation activity it harbors (e.g. Leurini et al. 2011a; König et al. 2017; Giannetti et al. 2017b). Around the hot-core, $f_D \lesssim 1.5$. In Fig. 2 we see that, when the temperature decreases, the value of f_D increases with $N(H_2)$, because, for the same temperature, the depletion is more efficient at large $n(H_2)$ (see eq. 1 and also Caselli et al. 1999 for more details). This result confirms the hypothesis that HMSFRs are more prone to show large-scale CO-depletion.

4. Depletion modeling

To compute the size of the depleted area, we built a simple 1D radial model and we applied it for three separate regions along the main-body, *viz.* regions C5, C7 and F1, associated, respectively, with clump-5, -7 and the filamentary region between them (see Fig. 1). We assumed a Plummer-like profile for the H_2 number density profile, as follows:

$$n(H_2) = n(H_{2,spine}) \left[1 + \left(\frac{R}{R_{flat}}\right)^{\alpha}\right]^{-p/2}, \qquad (3)$$

up to a maximum distance $R_{max} \sim 0.2$ pc, where $n(H_{2,spine})$ is the central volume density of H_2 with respect to which we normalize the theoretical profiles to match the observations, and R_{flat} is the distance relative to the spine within which the density profile remains roughly flat (i.e. $n(H_2, R_{flat}) = n(H_{2,spine})/2$ if $p = 2$). The profile described in eq. 3 has four free parameters: the two power-law indices (α and p), the normalization factor for the $n(H_2)$ profile and the position of R_{flat}.

We simulate the depletion effect inside/outside the depletion radius with a simple step-function where, for $R < R_{dep}$, $f_D = 10$ or ∞ and $\chi_{C^{18}O} = \chi^E_{C^{18}O}/f_D$, while for $R > R_{dep}$, $f_D = 1$ and $\chi_{C^{18}O} = \chi^E_{C^{18}O}$. For $R < R_{dep}$, the lower limit of $f_D = 10$ is motivated by the observational constraints for high-mass clumps, which in most cases show depletion values between 1 and 10 (beam- and l.o.s.-averaged; see Sect. 1). Instead, the choice of extending the model until reaching the theoretical condition of full depletion (i.e., $f_D = \infty$) is made to study the effect that such a drastic variation of f_D has on the size of R_{dep}.

For reasons of space, here we will only show the results for clump-5. The complete description of the results can be found in Sabatini et al. (2019). However, we note that the results for the other regions, the derived R_{dep} are within a factor of 1.5 of those shown here.

In the best-fit model, we assumed $p = 2$ and eq. (3) takes the functional form described by Tafalla et al. (2002), while $\alpha = 1.9$ and R_{flat}=5.5×10^{-3} pc, as result of the fit. The value of α was found by exploring the parameter space defined by the results of Beuther et al.

(2002), i.e. 1.1< α <2.1. In Fig. 3 (*i*) and (*ii*), we show the best-fitting mean radial column density profiles of N(H_2) and N($C^{18}O$), respectively, as a function of the projected distance from the centre (*R*) of clump-5. As dashed lines, we show the column density profiles before convolution with the telescope beam and, as solid lines, the profiles convolved with the *Herschel* beam at 500 μm (i.e. 36 arcsec). The observed data are plotted as black points. In Fig. 3 (*iii*), we report the depletion factor as a function of *R*, assuming f_D = 10 for $R < R_{dep}$ (dashed line), or $f_D = \infty$ (solid line).

The estimated R_{dep} ranges between a minimum of ~0.07 pc and a maximum of ~0.10 pc. At these distances, the volume densities of H_2 are 5.7×10^4 cm^{-3} and 3.1×10^4 cm^{-3}, if $f_D = \infty$ or 10 for R< R_{dep}, respectively.

If we assume an axisymmetric distribution of the gas in the main-body and we take into account the width of the filament estimated from the $C^{18}O$(2-1) map (i.e. 0.37 ± 0.06 pc; L19), this result suggests that in ~1/4 of the whole structure of G351 about 90% of CO (f_D = 10) or more, could be depleted.

5. Conclusion

We presented results of a study on the large-scale CO-depletion factor f_D and its variation in the IRDC G351.77-0.51. We used *Herschel* and LABOCA dust continuum data together with APEX J=(2-1) line observations of $C^{18}O$ and $C^{17}O$, taking into account opacity and saturation effects on the data to derive the f_D map (Fig. 1). The depletion factor reaches values as high as ~6 along the main-body and close to clump-3, whereas in lower density, higher temperatures structures f_D is close to 1 as expected. In many regions of the spine and the branches, the derived f_D makes it clear that, even in the less prominent structures, the depletion of CO can start to occur, showing values larger than ~2.5.

We constructed a simple 1D (toy-)model to estimate the size of the depletion radius R_{dep}, reproducing observed f_D profiles in two clumps along the main ridge and along the filament itself. The model suggests that R_{dep} ranges between 0.10 and 0.07 pc, by chang-

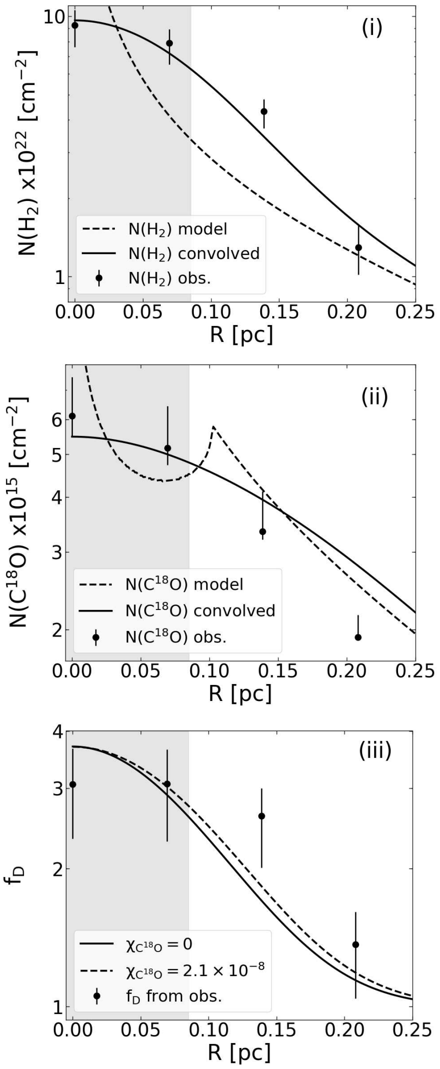

Fig. 3. Column densities N(H_2) and N($C^{18}O$) are plotted in panel (*i*) and (*ii*), respectively, as a function of the the projected distance from the centre (*R*) of clump-5. In panel (*iii*) we show the mean f_D profile in C5. Dashed-profiles show: the l.o.s.-integrated profiles of eq. 3 (panel *i*) and same for N($C^{18}O$) assuming f_D = 10 for R< R_{dep} (panel *ii*), while the R_{dep} position corresponds to the cusp; solid-drawn curves are the profiles convolved with the *Herschel* beam at 500μm (FWHM: grey-shaded area). Dashed- and solid-profiles in panel (*iii*), show the modeled f_D profiles. Black points are the observed values. The plots are adapted from Sabatini et al. (2019) and reprinted with permission.

ing the depletion degree from 10 to the full depletion state for $R < R_{dep}$. Assuming a cylindrically symmetric main-body, with a width of 0.37 ± 0.06 pc (L19), this result suggests that in ~1/4 of the volume of G351, about 90% of CO or more could be depleted.

For the future, higher resolution data will be important to test a family of the curves describing less drastic variation compared to the $C^{18}O/H_2$ profiles assumed in this work and to put stronger constraints on the estimated R_{dep} (see Sabatini et al. 2019).

Acknowledgements. This work is based on data acquired with the Atacama Pathfinder EXperiment (APEX). APEX is a collaboration between the Max Planck Institute for Radioastronomy, the European Southern Observatory, and the Onsala Space Observatory. This research made use of Astropy, a community-developed core Python package for Astronomy (Astropy Collaboration et al. 2013, 2018; see also `http://www.astropy.org`) and of NASAs Astrophysics Data System, of Matplotlib (Hunter 2007) and Pandas (McKinney 2010). SB acknowledges for funds through BASAL Centro de Astrofisica y Tecnologias Afines (CATA) AFB-17002, Fondecyt Iniciación (project code 11170268), and PCI Redes Internacionales para Investigadores(as) en Etapa Inicial (project number REDI170093). This research has made use of NASAs Astrophysics Data System Bibliographic Services (ADS).

References

Astropy Collaboration, Robitaille, T. P., Tollerud, E. J., et al. 2013, A&A, 558, A33
Astropy Collaboration, Price-Whelan, A. M., Sipőcz, B. M., et al. 2018, AJ, 156, 123
Bergin, E. A. & Tafalla, M. 2007, ARA&A, 45, 339
Beuther, H., Schilke, P., Menten, K. M., et al. 2002, ApJ, 566, 945
Caselli, P., et al. 1999, ApJ, 523, L165
Caselli, P., Vastel, C., Ceccarelli, C., et al. 2008, A&A, 492, 703
Crapsi, A., Caselli, P., Walmsley, C. M., et al. 2005, ApJ, 619, 379
Fontani, F., Giannetti, A., Beltrán, M. T., et al. 2012, MNRAS, 423, 2342
Giannetti, A., Wyrowski, F., Brand, J., et al. 2014, A&A, 570, A65
Giannetti, A., Leurini, S., König, C., et al. 2017a, A&A, 606, L12
Giannetti, A., Leurini, S., Wyrowski, F., et al. 2017b, A&A, 603, A33
Herbst, E. & van Dishoeck, E. F. 2009, ARA&A, 47, 427
Hernandez, A. K., Tan, J. C., Kainulainen, J., et al. 2012, ApJ, 756, L13
Hildebrand, R. H. 1983, QJRAS, 24, 267
Hunter, J. D. 2007, Computing In Science & Engineering, 9, 90
König, C., Urquhart, J. S., Csengeri, T., et al. 2017, A&A, 599, A139
Kramer, C. & Winnewisser, G. 1991, A&AS, 89, 421
Leurini, S., Codella, C., Zapata, L., et al. 2011a, A&A, 530, A12
Leurini, S., Pillai, T., Stanke, T., et al. 2011b, A&A, 533, A85
Leurini, S., Schisano, E., Pillai, T., et al. 2019, A&A, 621, A130
Li, G.-X., Urquhart, J. S., Leurini, S., et al. 2016, A&A, 591, A5
McKinney, W. 2010, in Proceedings of the 9th Python in Science Conference, ed. S. van der Walt & J. Millman, 51
Menten, K. M., Pillai, T., & Wyrowski, F. 2005, in Massive Star Birth: A Crossroads of Astrophysics, ed. R. Cesaroni, M. Felli, E. Churchwell, & M. Walmsley (Cambridge Univ. Press, Cambridge), IAU Symp., 227, 23
Sabatini, G., Giannetti, A., Bovino, S., et al. 2019, MNRAS, 490, 4489
Schuller, F., Menten, K. M., Contreras, Y., et al. 2009, A&A, 504, 415
Tafalla, M., Myers, P. C., Caselli, P., Walmsley, C. M., & Comito, C. 2002, ApJ, 569, 815
Wouterloot, J. G. A., Henkel, C., Brand, J., & Davis, G. R. 2008, A&A, 487, 237
Zinnecker, H. & Yorke, H. W. 2007, ARA&A, 45, 481